Thermochimica Acta 479 (2008) 1–6

Contents lists available at ScienceDirect

Thermochimica Acta

journal homepage: www.elsevier.com/locate/tca

Thermal decomposition of synthesised layered double hydroxides based upon Mg/(Fe,Cr) and carbonate

Henry J. Spratt, Sara J. Palmer, Ray L. Frost*

Inorganic Materials Research Program, School of Physical and Chemical Sciences, Queensland University of Technology, GPO Box 2434, Brisbane, Queensland 4001, Australia

ARTICLE INFO

Article history:
Received 29 April 2008
Received in revised form 27 August 2008
Accepted 29 August 2008
Available online 7 September 2008

Keywords:
Hydrotalcite
Pyroaurite
Carbonate
X-ray diffraction
Thermal analysis

ABSTRACT

Thermal analysis complimented with evolved gas mass spectrometry has been applied to hydrotalcites of the pyroaurite–stitchtite series containing the carbonate anion prepared by co-precipitation and with varying Fe^{3+}, Cr^{3+} trivalent cation ratio. The resulting materials were characterised by XRD, and TGA/DTG to determine the stability of the hydrotalcites synthesised. Hydrotalcites of formula $Mg_6(Cr_{0.8},Fe_{0.2})_2(OH)_{16}(CO_3)\cdot xH_2O$, $Mg_6(Cr_{0.6},Fe_{0.4})_2(OH)_{16}(CO_3)\cdot xH_2O$, $Mg_6(Cr_{0.4},Fe_{0.6})_2(OH)_{16}(CO_3)\cdot xH_2O$ and $Mg_6(Cr_{0.2},Fe_{0.8})_2(OH)_{16}(CO_3)\cdot xH_2O$ formed by intercalation with the carbonate anion as a function of Fe^{3+}, Cr^{3+} trivalent cationic ratio show variation in the *d*-spacing attributed to the size of the cation.

The thermal decomposition of stitchtite–pyroaurite solid solution follows the following steps:

(a) removal of adsorbed water (<100 °C),
(b) elimination of the interlayer structural water (100–150 °C), and
(c) the simultaneous dehydroxylation and decarbonation of the hydrotalcite framework (300–400 °C).

The effect of replacement of Cr^{3+} by Fe^{3+} has no effect on the dehydroxylation temperature. The ion current curves provide evidence for the formation of Fe^{3+} and Cr^{3+} carbonates during dehydroxylation. Dehydroxylation results in the collapse of the hydrotalcite structure to that of its corresponding metal oxides, and results in the formation of spinels, including MgO, $MgFe_2O_4$, $MgCr_2O_4$, and $MgFeAlO_4$.

1. Introduction

Hydrotalcites, or layered double hydroxides (LDHs) are fundamentally anionic clays, and are less well-known than cationic clays like smectites [1,2]. The structure of hydrotalcite can be derived from a brucite structure ($Mg(OH)_2$) in which e.g. Al^{3+} or Fe^{3+} (pyroaurite–sjögrenite) substitutes for Mg^{2+} [3–14]. This substitution creates a positive layer charge on the hydroxide layers, which is compensated by interlayer anions or anionic complexes [15,16]. When LDHs are synthesised any appropriate anion can be placed in the interlayer. These anions may be any anion with a suitable negative charge including the phosphate anion. The hydrotalcite may be considered as a gigantic cation which is counterbalanced by anions in the interlayer. In hydrotalcites a broad range of compositions are possible of the type $[M_{1-x}^{2+}M_x^{3+}(OH)_2][A^{n-}]_{x/n}\cdot yH_2O$, where M^{2+} and M^{3+} are the di- and trivalent cations in the octahedral positions within the hydroxide layers with *x* normally between 0.17 and 0.33. It is a normal practice to determine the composition of the formed hydrotalcite by chemical means such as ICP-AES or EDAX techniques. A^{n-} is an exchangeable interlayer anion [17]. In the hydrotalcites pyroaurite and stitchtite, the di-valent cation is Mg^{2+} with the trivalent cation being Fe^{3+} and Cr^{3+}, respectively. In these cases, the carbonate anion is the major interlayer counter anion. Normally the hydrotalcite structure based upon hydrotalcite (Mg, Al) has basal spacings of ~8.0 Å where the interlayer anion is carbonate [18,19].

Thermal analysis using thermogravimetric techniques enables the mass loss steps, the temperature of the mass loss steps and the mechanism for the mass loss to be determined [6,11,20–24]. Thermoanalytical methods provide a measure of the thermal stability of the hydrotalcite. The reason for the potential application of hydrotalcites as catalysts rests with the ability to make mixed metal oxides at the atomic level, rather than at a particle level. Such mixed metal oxides are formed through the thermal decomposition of the hydrotalcite [25,26]. There are many other important uses of hydrotalcites such as in the removal of environmental hazards in

* Corresponding author. Tel.: +61 7 3138 2407; fax: +61 7 3138 1804.
E-mail address: r.frost@qut.edu.au (R.L. Frost).

0040-6031/$ – see front matter © 2008 Elsevier B.V. All rights reserved.
doi:10.1016/j.tca.2008.08.016

acid mine drainage [27,28], and a mechanism for the disposal of radioactive wastes [29]. Their ability to exchange anions presents a system for heavy metal removal from contaminated waters [30]. Structural information on different minerals has successfully been obtained recently by sophisticated thermal analysis techniques [6,20–24].

In this work we report the thermal analysis of (Fe^{3+}, Cr^{3+}) hydrotalcites with carbonate in the interlayer and explore the effect of (Fe^{3+}, Cr^{3+}) ratio on hydrotalcite formation and explore the thermal stability of these hydrotalcites. Fundamentally these synthesised hydrotalcites are solid solutions of pyroaurite–stitchtite. Thermal analysis has proven most useful for the study of the thermal stability of hydrotalcites [11,31–34]. The objective of this research is to determine the thermal stability of hydrotalcites synthesised with different trivalent Fe^{3+}/Cr^{3+} cationic ratios.

2. Experimental

2.1. Synthesis and characterisation of Mg, Fe(III), Cr(III) hydrotalcites with varying Fe/Cr ratios

A caustic solution (8 g NaOH and 3.2 g Na_2CO_3 at 100 mL) was stirred vigorously at 65 °C, while 100 mL of the mixed metal ion solution ($Mg(NO_3)_3{\cdot}6H_2O$, $Fe(NO_3)_3{\cdot}6H_2O$ and $Cr(NO_3)_3{\cdot}9H_2O$), is added dropwise to the caustic solution. The following table indicates the moles of each metal nitrate used.

Ratio (Cr:Fe)	Moles of Mg nitrate	Moles of Fe(III) nitrate	Moles of Cr(III) nitrate	Sample number
0.8:0.2	0.075	0.005	0.02	1-Mg, Fe, Cr LDH
0.6:0.4	0.075	0.01	0.015	2-Mg, Fe, Cr LDH
0.4:0.6	0.075	0.015	0.01	3-Mg, Fe, Cr LDH
0.2:0.8	0.075	0.02	0.005	4-Mg, Fe, Cr LDH

The resulting solution was aged at 65 °C for 18–20 h, filtered with hot and cold water to remove nitrates and dried in an oven overnight at 65 °C.

2.2. X-ray diffraction

X-ray diffraction patterns were collected using a Philips X'pert wide angle X-ray diffractometer, operating in step scan mode, with Cu Kα radiation (1.54052 Å). Patterns were collected in the range 3–90° 2θ with a step size of 0.02° and a rate of 30 s per step. Samples were prepared as a finely pressed powder into aluminium sample holders. The Profile Fitting option of the software uses a model that employs twelve intrinsic parameters to describe the profile, the instrumental aberration and wavelength-dependent contributions to the profile.

2.3. Thermal analysis

Thermal decomposition of the hydrotalcite was carried out in a TA® Instruments incorporated high-resolution thermogravimetric analyzer (series Q500) in a flowing nitrogen atmosphere (80 cm^3/min). Approximately 50 mg of sample was heated in an open platinum crucible at a rate of 5.0 °C/min up to 1000 °C at high resolution. With the quasi-isothermal, quasi-isobaric heating program of the instrument the furnace temperature was regulated precisely to provide a uniform rate of decomposition in the main decomposition stage. The TGA instrument was coupled to a Balzers (Pfeiffer) mass spectrometer for gas analysis. Only selected gases such as water and carbon dioxide were analyzed.

3. Results and discussion

3.1. X-ray diffraction

The X-ray diffraction patterns for the carbonate interlayer hydrotalcites are shown in Fig. 1. Hydrotalcite normally has a d(0 0 3) spacing of around 7.9 Å. The XRD patterns obtained for the synthetic hydrotalcites match closely with reference pattern 01-070-2150 (pyroaurite—$(Fe_2Mg_6(OH)_{16}CO_3(H_2O)_{4.5})_{0.375}$). The method of synthesis for these hydrotalcites allows for the possibility of a variety of products including: hydrotalcite, pyroaurite, stitchtite and other forms of hydrotalcites with a mixture of cationic ratios. However, there appears to be only one phase present in the XRD pattern, suggesting that other phases were not produced. Minor quantities may have been produced but were not detected using XRD. The d(0 0 3) obtained for the synthesised 1, 2, 3, and 4 hydrotalcites is 7.656, 7.921, 7.766, and 7.955 Å, respectively. The XRD pattern of the decomposed products of the LDHs identified spinel and mixed oxides, Fig. 1b, thus confirming the dehydroxylation and decarbonation of these structures.

The shape of the d(1 1 0) peak becomes more defined as the quantity of Fe^{3+} in the LDH structure increases. In the 1-Mg, Fe, Cr LDH, the d(1 1 0) and d(1 1 3) spacing peak merge together to form one broad peak. This broadness suggests that the LDHs with a lower content of Fe^{3+} forms particles with smaller domain sizes then those with more Fe^{3+} in the structure. Variation in the d(1 1 0) spacing is observed as the Fe^{3+} is replaced by Cr^{3+} the 1 1 0 reflection increases as the two ions Cr^{3+} and Fe^{3+} have different ionic radii. The ionic radii of Fe^{3+} (CN = 4, HS): 0.63 Å, Fe^{3+} (CN = 6, LS): 0.69 Å, Fe^{3+} (CN = 6, HS): 0.79 Å and Cr^{3+} (CN = 6): 0.76 Å. The 1 1 0 spacing is as follows: 1-Mg, Fe, Cr LDH: 1.542 Å; 2-Mg, Fe, Cr LDH: 1.555 Å; 3-Mg, Fe, Cr LDH: 1.554 Å and 4-Mg, Fe, Cr LDH: 1.554 Å. The d(1 1 0) spacing reduced slightly for the LDH with Cr:Fe ratio 4:1.

3.2. Thermogravimetry

3.2.1. Thermal decomposition of $Mg_6(Cr_{0.8},Fe_{0.2})_2(OH)_{16}(CO_3){\cdot}xH_2O$ layered double hydroxide

The TG and DTG curves for the synthesised 1-Mg(Fe,Cr) LDH (Cr:Fe = 0.7:0.2) are shown in Fig. 2a and the gas evolution ion current curves resulting from the thermal decomposition in Fig. 3a. Two major mass loss steps are observed at 60 and 347 °C with a third mass loss step at 395 °C. The mass losses observed at these temperatures are 16.2, 22.5 and 6.0%. The first mass loss step is attributed to dehydration. The following reaction is proposed:

$$Mg_6(Cr_{0.8}, Fe_{0.2})_2(OH)_{16}(CO_3){\cdot}xH_2O \rightarrow Mg_6(Cr_{0.8}, Fe_{0.2})_2(OH)_{16}(CO_3) + xH_2O.$$

The ion current curves show a maximum for the m/z ratios of 17 and 18 at 61 °C. The dehydration mass loss step is highly asymmetric and stretches out to 150 °C. Thus this mass loss step includes not only dehydration but removal of the interlayer water as well.

The mass loss step at 347 °C is assigned to a combination of dehydration and decarbonation which appear to occur simultaneously. The ion current curves for m/z = 44 (CO_2) prove that CO_2 is lost at 351 and 393 °C. According to the ion current curves, no CO_2 is lost at temperatures lower than 351 °C. It is possible that the formation of carbonates is an intermediate step in the dehydroxylation/decarbonation step, which is seen at these higher decomposition temperatures. The ion current curves for m/z = 17 and 18 show that water vapour is evolved at 348 °C. The ion current curves show that oxygen is lost during the thermal transformation at 348 °C. However, minimal water vapour is lost at 393 °C. The

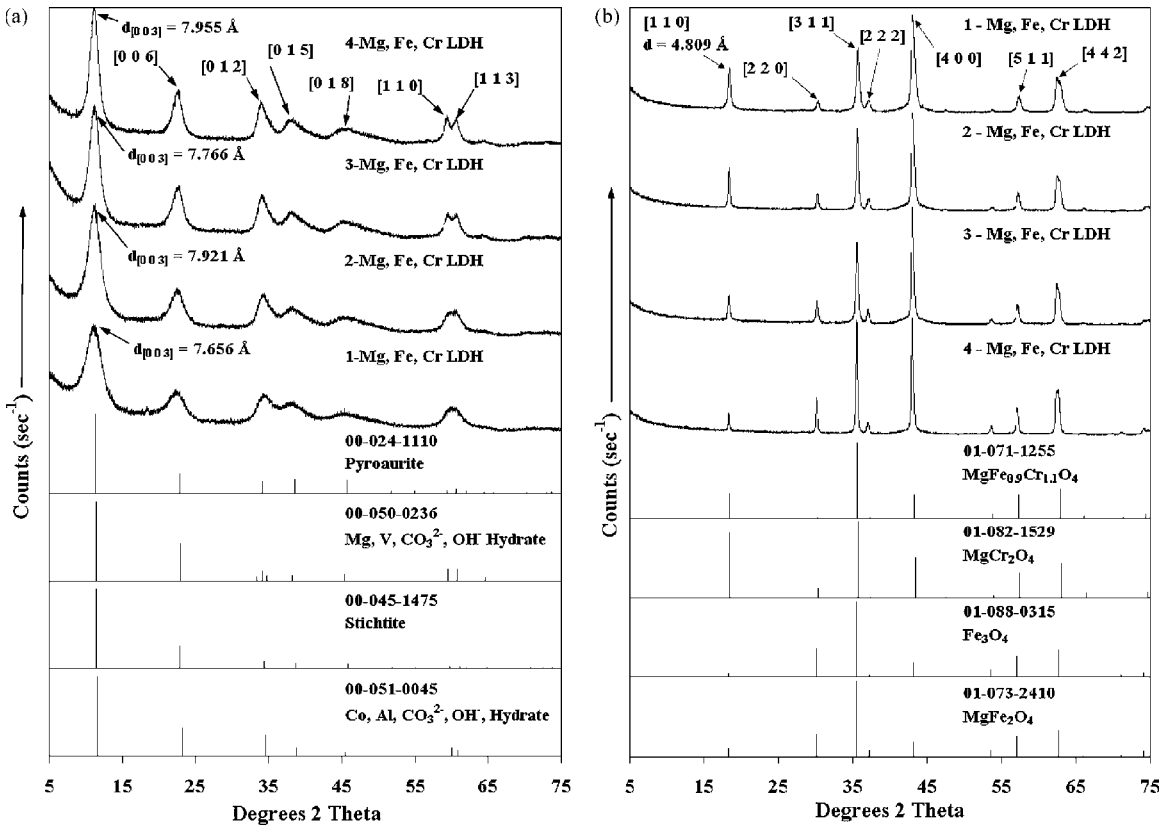

Fig. 1. (a) X-ray diffraction patterns of Mg(Fe,Cr) LDH and the reference patterns. (b) X-ray diffraction patterns of decomposition products of Mg(Fe,Cr) LDH and their reference patterns.

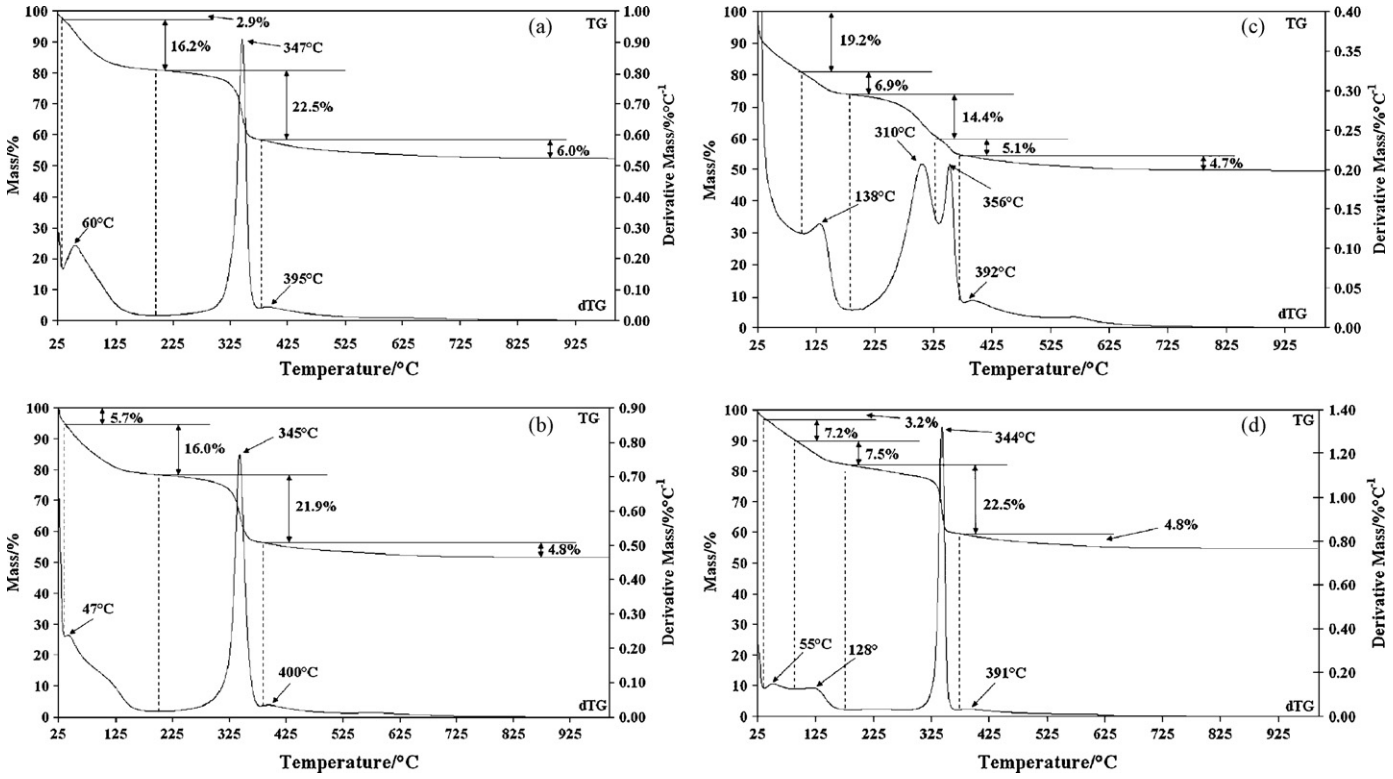

Fig. 2. (a) Thermogravimetric and differential thermogravimetric analysis of 1-Mg(Fe,Cr) LDH. (b) Thermogravimetric and differential thermogravimetric analysis of 2-Mg(Fe,Cr) LDH. (c) Thermogravimetric and differential thermogravimetric analysis of 3-Mg(Fe,Cr) LDH. (d) Thermogravimetric and differential thermogravimetric analysis of 4-Mg(Fe,Cr) LDH.

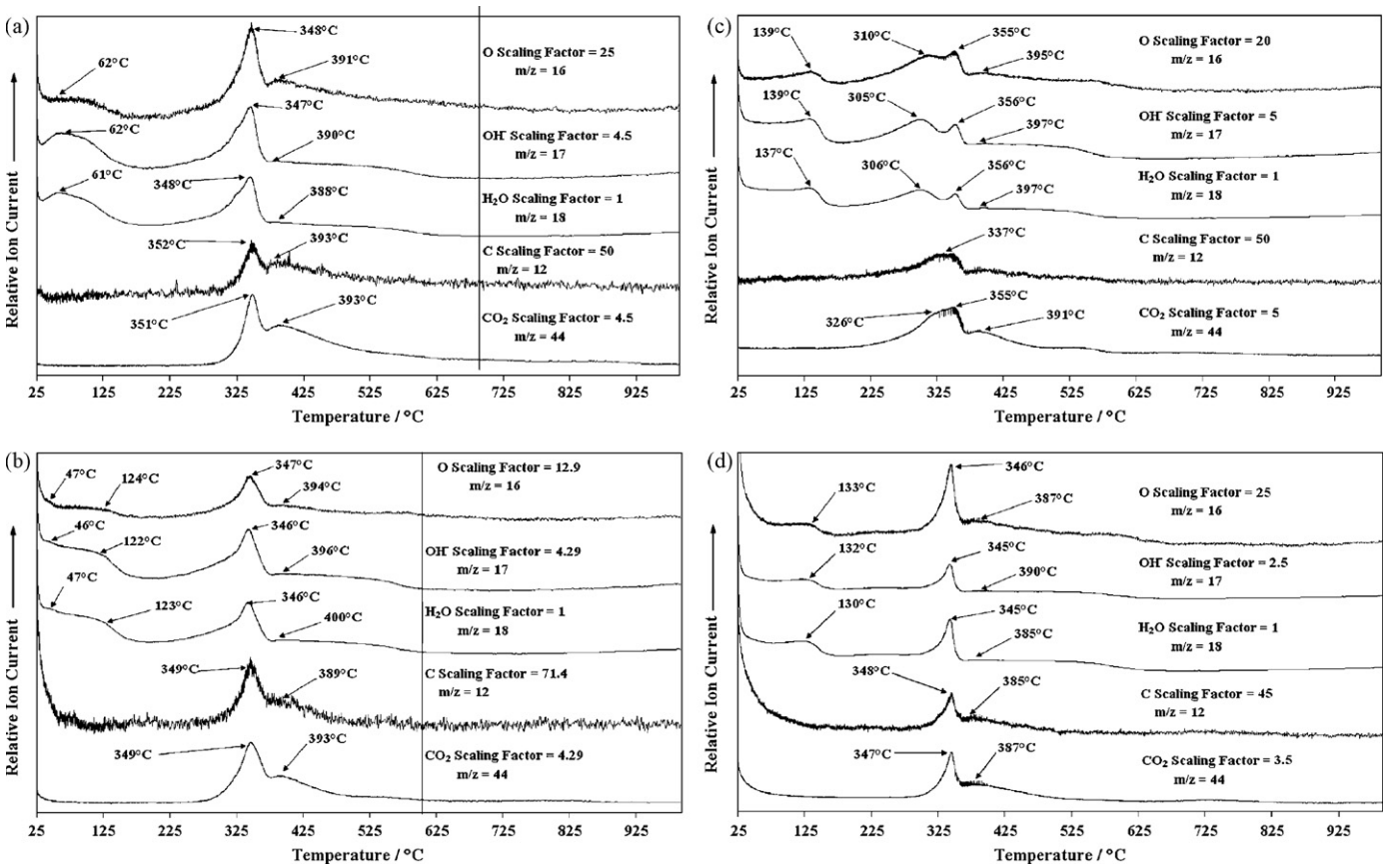

Fig. 3. (a) Ion current curves for the gas evolution analysis of 1-Mg(Fe,Cr) LDH. (b) Ion current curves for the gas evolution analysis of 2-Mg(Fe,Cr) LDH. (c) Ion current curves for the gas evolution analysis of 3-Mg(Fe,Cr) LDH. (d) Ion current curves for the gas evolution analysis of 4-Mg(Fe,Cr) LDH.

following reaction is proposed for the decomposition of the LDH structure:

$$Mg_6(Cr_{0.8}, Fe_{0.2})_2(OH)_{16}(CO_3) \rightarrow 0.2MgFe_2O_4 + 0.8MgCr_2O_4 + 5MgO + CO_2 + 8H_2O$$

The molecular mass of $Mg_6(Cr_{0.8},Fe_{0.2})_2(OH)_{16}(CO_3)$ is 581.8. Thus the theoretical mass loss for dehydroxylation and decarbonation is 24.8 and 7.6%, respectively. These values resemble closely to the values reported in Fig. 2a. Based on the theoretical calculations, it appears that the majority of decarbonation occurs at 393 °C, which showed a mass loss of 6.0%. Therefore, the peak at 347 °C is primarily due to dehydroxylation.

3.2.2. Thermal decomposition of $Mg_6(Cr_{0.6},Fe_{0.4})_2(OH)_{16}(CO_3)\cdot xH_2O$ layered double hydroxide

The thermal decomposition of the $Mg_6(Cr_{0.6},Fe_{0.4})_2(OH)_{16}(CO_3)\cdot xH_2O$ layered double hydroxide is shown in Fig. 2b and the associated ion current curves are reported in Fig. 3b. Four mass loss steps are observed: (a) up to 47 °C, (b) from 47 to 150 °C, (c) at 345 °C, and (d) at 400 °C. These mass loss steps are attributed to: (a) the loss of adsorbed water, (b) dehydration, (c) dehydroxylation and decarbonation, and (d) decarbonation. The mass losses for these steps are 5.7, 16.0, 21.9 and 4.8%, respectively. The following reactions are proposed:

Dehydration up to 150 °C:

$$Mg_6(Cr_{0.6}, Fe_{0.4})_2(OH)_{16}(CO_3)\cdot xH_2O \rightarrow Mg_6(Cr_{0.6}, Fe_{0.4})_2(OH)_{16}(CO_3) + xH_2O$$

Dehydroxylation at 345 °C:

$$Mg_6(Cr_{0.6}, Fe_{0.4})_2(OH)_{16}(CO_3) \rightarrow Mg_6O_8(Cr_{0.6}, Fe_{0.4})_2(CO_3) + 8H_2O$$

Decarbonation at 345 and 400 °C:

$$Mg_6O_8(Cr_{0.6}, Fe_{0.4})_2(CO_3) \rightarrow 0.4MgFe_2O_4 + 0.6MgCr_2O_4 + 5MgO + CO_2$$

The ion current curves for $m/z = 17$ and 18 prove the loss of water up to 125 °C and the loss of water vapour at 346 °C is due to the dehydroxylation process. The ion current curve for $m/z = 44$ shows that CO_2 is lost at 349 and 393 °C. This result suggests that not all the CO_2 is lost at 349 °C. The theoretical mass loss of CO_2 is 7.5%. The results show a mass loss of 4.8% at 400 °C, which suggests that 2.7% of the theoretical CO_2 is lost at 346 °C. The ion current curves prove that no OH units are retained after 349 °C. Thus it is proposed that some carbonate formation results from the dehydroxylation of the hydrotalcite. It is possible that $Fe_2(CO_3)_3$ and $Cr_2(CO_3)_3$ are formed and if some reduction occurs then $FeCO_3$ and $CrCO_3$ may be formed. Thus at 393 °C these carbonates decompose.

3.2.3. Thermal decomposition of $Mg_6(Cr_{0.4},Fe_{0.6})_2(OH)_{16}(CO_3)\cdot xH_2O$ layered double hydroxide

The thermal decomposition of the $Mg_6(Cr_{0.4},Fe_{0.6})_2(OH)_{16}(CO_3)\cdot xH_2O$ layered double hydroxide and the associated ion current curves provide information on the thermal decomposition of this stitchtitepyroaurite (Figs. 2c and 3c). The thermal decomposition behaviour of this system is very different from the previous two synthesised Fe/Cr hydrotalcites. Five mass loss steps are observed:

(a) up to 50 °C, (b) from 50 to 150 °C, (c) at 310 °C, (d) at 346 °C, and (e) at 400 °C. These mass loss steps are attributed to: (a) the loss of adsorbed water, (b) dehydration, (c) dehydroxylation, (d) dehydroxylation and decarbonation, and (e) decarbonation. The mass losses for these steps are 19.2, 6.9, 14.4, 5.1, and 4.7%, respectively. In this hydrotalcite, the mass loss approaching 26% is attributed to the loss of adsorbed water. This value is considerably higher than in the other studied systems. The question arises as to why is this so. The XRD patterns clearly show that a normal regular LDH is formed. Yet the thermal analysis pattern is very different. It is proposed that the stacking of the LDH layers is different and that there may be some displacement of the layers making the material mesoporous resulting in the uptake of more water. Such a proposition requires more research to validate these statements.

The following reactions are proposed:

Dehydration up to 150 °C:

$$Mg_6(Cr_{0.4}, Fe_{0.6})_2(OH)_{16}(CO_3)\cdot xH_2O \rightarrow Mg_6(Cr_{0.4}, Fe_{0.6})_2(OH)_{16}(CO_3) + xH_2O$$

Dehydroxylation at 345 °C:

$$Mg_6(Cr_{0.4}, Fe_{0.6})_2(OH)_{16}(CO_3) \rightarrow Mg_6O_8(Cr_{0.4}, Fe_{0.6})_2(CO_3) + 8H_2O$$

Decarbonation at 345 and 400 °C:

$$Mg_6O_8(Cr_{0.4}, Fe_{0.6})_2(CO_3) \rightarrow 0.6MgFe_2O_4 + 0.4MgCr_2O_4 + 5MgO + CO_2$$

The ion current curves for $m/z = 17$ and 18 prove the loss of water up to around 138 °C and the loss of water vapour through the dehydroxylation process at 310 and 346 °C. The overall shape of the DTG is considerably different from the other three LDHs structures being investigated. The ion current curve shows the loss of OH and H_2O units, $m/z = 17$ and 18 respectively, occurs at two defined temperatures: 306 and 356 °C. This is also observed in the DTG curve with two distinct peaks being observed at 310 and 356 °C. Therefore, it is suggested that the $Mg_6(Cr_{0.4},Fe_{0.6})_2(OH)_{16}(CO_3)\cdot xH_2O$ LDH is thermally less stable then the other LDHs synthesised, due to this initial dehydroxylation step at 306 °C. The absence of peaks after 356 °C for $m/z = 17$ and 18 in the ion current curve, indicates the complete dehydroxylation of the structure at this temperature. The peak at 356 °C is due to the simultaneous dehydroxylation and decarbonation of the LDH structure, shown by the evolution of both OH units and CO_2, at 355 °C on the ion current curve. The ion current curve for $m/z = 44$ shows that CO_2 is also lost at 393 °C. It is proposed that this mass loss is due to the decomposition of carbonate species, such as $Fe_2(CO_3)_2$ and $Cr_2(CO_3)_2$, which forms during the dehydroxylation of the LDH structure.

3.2.4. Thermal decomposition of $Mg_6(Cr_{0.2},Fe_{0.8})_2(OH)_{16}(CO_3)\cdot xH_2O$ layered double hydroxide

The thermal decomposition of $Mg_6(Cr_{0.2},Fe_{0.8})_2(OH)_{16}(CO_3)\cdot xH_2O$ layered double hydroxide is reported in Fig. 2d and the appropriate selected ion current curves in Fig. 3d. In the DTG pattern four mass loss steps are resolved at 55, 128, 344 and 391 °C with mass losses of 7.2, 7.5, 22.5 and 4.8%. The first two steps are attributed to dehydration, the third step to dehydroxylation and decarbonation and the four mass loss step to partial decarbonation. It is noted that some distinction between the loss of adsorbed water and intercalated water is resolved in this DTG pattern, with distinct peaks being observed at 55 and 128 °C. The dehydroxylation and decarbonation of this LDH structure, resembles the LDH structures: $Mg_6(Cr_{0.8},Fe_{0.2})_2(OH)_{16}(CO_3)\cdot xH_2O$ and $Mg_6(Cr_{0.6},Fe_{0.4})_2(OH)_{16}(CO_3)\cdot xH_2O$, with approximately the same mass losses being observed. It is noted that as the Fe^{3+} replaces the Cr^{3+} in the pyroaurite–stitchtite hydrotalcites almost no shift in the dehydroxylation temperature occurs, except the $Mg_6(Cr_{0.4},Fe_{0.6})_2(OH)_{16}(CO_3)\cdot xH_2O$. Therefore, the thermal stability remains relatively constant over these varying trivalent cationic ratios.

4. Conclusions

Hydrotalcites of the stitchtite–pyroaurite series were synthesised and characterised by powder X-ray diffraction and thermogravimetry with mass spectrometry. The different LDHs show some variation in the *d*-spacing attributed to the size of the cation. This is observed in the change in position of the 1 1 0 reflection as the Fe^{3+} is replaced with Cr^{3+}.

The decomposition of the synthesised hydrotalcites occurred in four steps: (1) evapouration of adsorbed water (up to 100 °C), (2) elimination of the interlayer structural water (up to 200 °C), (3) dehydroxylation and decarbonation of the hydrotalcite framework (up to 350 °C), and (4) decarbonation (up to 400 °C). The ion current curve revealed that a small proportion of the dehydroxylation and decarbonation process occurred simultaneously. The ion current curves provide some evidence for the formation of intermediates in the dehydroxylation process resulting in the formation of some carbonates, which are retained at slightly higher temperatures.

The dehydroxylation temperature indicates the thermal stability of the hydrotalcite structure, where delays in dehydroxylation indicate a more stable hydrotalcite. Limited differences were observed for these synthesised stitchtite–pyroaurite solid solutions. The $Mg_6(Cr_{0.4},Fe_{0.6})_2(OH)_{16}(CO_3)\cdot xH_2O$ showed a different DTG compared to the other LDHs synthesised, where the dehydroxylation and decarbonation peaks are more defined, clearly showing the initial dehydroxylation at 310 °C, followed by the final dehydroxylation and partial decarbonation at 356 °C. The collapse of the hydrotalcite structure produced corresponding metal oxides and spinels, including $MgCr_2O_4$, $MgFe_2O_4$ and $MgFeAlO_4$.

Acknowledgements

The financial and infra-structure support of the Queensland Research and Development Centre (QRDC-Alcan) and the Queensland University of Technology Inorganic Materials Research Program of the School of Physical and Chemical Sciences is gratefully acknowledged. One of the authors (SJP) is grateful to Alcan for a Masters scholarship. The Australian Research Council (ARC) is thanked for funding the Thermal Analysis Facility.

References

[1] K. Hashi, S. Kikkawa, M. Koizumi, Clay. Clay Miner. 31 (1983) 152–154.
[2] L. Ingram, H.F.W. Taylor, Mineral. Mag. J. Mineral. Soc. (1876–1968) 36 (1967) 465–479.
[3] J.T. Kloprogge, L. Hickey, R.L. Frost, Mater. Chem. Phys. 89 (2005) 99–109.
[4] L. Frost Ray, L. Erickson Kristy, Spectrochim. Acta A: Mol. Biomol. Spectrosc. 61 (2005) 51–56.
[5] K.L. Erickson, T.E. Bostrom, R.L. Frost, Mater. Lett. 59 (2004) 226–229.
[6] R.L. Frost, K.L. Erickson, J. Therm. Anal. Calorim. 76 (2004) 217–225.
[7] R.L. Frost, K.L. Erickson, Thermochim. Acta 421 (2004) 51–58.
[8] J.T. Kloprogge, L. Hickey, R.L. Frost, J. Raman Spectrosc. 35 (2004) 967–974.
[9] J.T. Kloprogge, L. Hickey, R.L. Frost, J. Solid State Chem. 177 (2004) 4047–4057.
[10] R.L. Frost, Z. Ding, Thermochim. Acta 405 (2003) 207–218.
[11] R.L. Frost, W. Martens, Z. Ding, J.T. Kloprogge, J. Therm. Anal. Calorim. 71 (2003) 429–438.
[12] R.L. Frost, M.L. Weier, M.E. Clissold, P.A. Williams, Spectrochim. Acta A 59 (2003) 3313–3319.
[13] R.L. Frost, M.L. Weier, M.E. Clissold, P.A. Williams, J.T. Kloprogge, Thermochim. Acta 407 (2003) 1–9.
[14] R.L. Frost, M.L. Weier, J.T. Kloprogge, J. Raman Spectrosc. 34 (2003) 760–768.
[15] R.M. Taylor, Clay Miner. 17 (1982) 369–372.

[16] H.F.W. Taylor, Mineral. Mag. J. Mineral. Soc. (1876–1968) 37 (1969) 338–342.
[17] H.C.B. Hansen, C.B. Koch, Appl. Clay Sci. 10 (1995) 5–19.
[18] D.L. Bish, A. Livingstone, Mineral. Mag. 44 (1981) 339–343.
[19] E.H. Nickel, R.M. Clarke, Am. Mineral. 61 (1976) 366–372.
[20] E. Horvath, J. Kristof, R.L. Frost, N. Heider, V. Vagvoelgyi, J. Therm. Anal. Calorim. 78 (2004) 687–695.
[21] R.L. Frost, M.L. Weier, K.L. Erickson, J. Therm. Anal. Calorim. 76 (2004) 1025–1033.
[22] R.L. Frost, K.L. Erickson, J. Therm. Anal. Calorim. 78 (2004) 367–373.
[23] E. Horvath, J. Kristof, R.L. Frost, A. Redey, V. Vagvolgyi, T. Cseh, J. Therm. Anal. Calorim. 71 (2003) 707–714.
[24] J. Kristof, R.L. Frost, J.T. Kloprogge, E. Horvath, E. Mako, J. Therm. Anal. Calorim. 69 (2002) 77–83.
[25] F. Rey, V. Fornes, J.M. Rojo, J. Chem. Soc., Faraday Trans. 88 (1992) 2233–2238.
[26] M. Valcheva-Traykova, N. Davidova, A. Weiss, J. Mater. Sci. 28 (1993) 2157–2162.
[27] G. Lichti, J. Mulcahy, Chem. Aust. 65 (1998) 10–13.
[28] Y. Seida, Y. Nakano, J. Chem. Eng. Japan 34 (2001) 906–911.
[29] Y. Roh, S.Y. Lee, M.P. Elless, J.E. Foss, Clay. Clay Miner. 48 (2000) 266–271.
[30] Y. Seida, Y. Nakano, Y. Nakamura, Water Res. 35 (2001) 2341–2346.
[31] J. Bouzaid, R.L. Frost, J. Therm. Anal. Calorim. 89 (2007) 133–135.
[32] J.M. Bouzaid, R.L. Frost, W.N. Martens, J. Therm. Anal. Calorim. 89 (2007) 511–519.
[33] R.L. Frost, A.W. Musumeci, M.O. Adebajo, W. Martens, J. Therm. Anal. Calorim. 89 (2007) 95–99.
[34] R.L. Frost, J.M. Bouzaid, A.W. Musumeci, J.T. Kloprogge, W.N. Martens, J. Therm. Anal. Calorim. 86 (2006) 437–441.